J Appl Electrochem (2013) 43:939–951
DOI 10.1007/s10800-013-0579-5

ORIGINAL PAPER

Synthesis of imidazole-based NHC–Au(I) complexes and their application in non-enzymatic glucose sensing

M. U. Anu Prathap · Carlos Alberto Huerta Aguilar · Thangarasu Pandiyan · Rajendra Srivastava

Received: 2 April 2013 / Accepted: 25 June 2013 / Published online: 10 July 2013

Abstract In this study, imidazole-based NHC–Au(I) complexes were prepared. Geometrically optimized structures and molecular orbital energy diagrams were computed using density functional theory. Cyclic voltammetry and amperometric methods were used to evaluate the catalytic activity of the NHC–Au(I)-modified electrodes toward glucose oxidation. The mechanism of electrocatalytic oxidation at NHC–Au(I)-modified electrodes is explained on the basis of the oxidation and reduction potentials in the presence of glucose. Applicability of NHC–Au(I)-modified electrode was extended to determine the glucose level in the blood serum and the precision of the method was found to be satisfactory. The non-enzymatic sensor exhibited excellent reproducibility, repeatability, antifouling, and anti-interference characteristics.

Keywords NHC–Au(I) complex · Glucose · Electrochemistry · Non-enzymatic sensor · DFT

1 Introduction

The development of fast and reliable method for glucose determination is essential in many areas such as clinical diagnostics, food industry, and sustainable fuel cells (microbial fuel cell [MFC]) [1–3]. Common glucose biosensors are based on enzyme. Numerous reports are available, which deal with the glucose oxidase (GO_x)-modified electrodes [4–8]. However, significant loss in activity of glucose oxidase (GO_x)-modified electrode is observed due to their immobilization in various matrixes and long-term instability, which cause loss in their sensitivity and reproducibility [6–14]. Therefore, considerable attention has been paid to develop non-enzymatic sensors for glucose detection [9–11]. Pt-modified electrodes were found to be the most appropriate for the electrochemical oxidation of glucose [12, 15]. However, low sensitivity, poisoning by adsorbed intermediates, and poor selectivity of Pt-based electrodes have attracted significant attention to look for alternative electrode materials [12, 15].

Another important Nobel metal, gold (Au) is known for its medicinal value from ancient time [16, 17]. Gold has received much interest because of their applications in catalysis, nanoelectronics, drug delivery, and chemical sensing [16–21]. Au can exist in a number of oxidation states. However, only Au(0), Au(I), and Au(III) are stable in aqueous solution [17, 22]. Au activity is strongly influenced by the pH and the composition of the electrolyte solution. It has been demonstrated that Au-catalyzed glucose oxidation takes place more efficiently in the alkaline medium (pH $\geq$ 11) [23]. The mechanism of electrocatalytic glucose oxidation on Au electrode consists of fast chemisorptions of glucose on the electrode, followed by dehydrogenation and simultaneous decomposition of the organic molecule [24, 25]. Au(I) complex-based chemosensing is widely investigated [26]. The exploration and development of Au(I) chemistry represents a fascinating and challenging area, and has attracted growing interest during the last two decades [26]. We recently reported the

Electronic supplementary material The online version of this article (doi:10.1007/s10800-013-0579-5) contains supplementary material, which is available to authorized users.

M. U. Anu Prathap · R. Srivastava (✉)
Department of Chemistry, Indian Institute of Technology Ropar, Rupnagar 140001, India
e-mail: rajendra@iitrpr.ac.in

C. A. H. Aguilar · T. Pandiyan (✉)
Faculty of Chemistry, National Autonomous University of Mexico (UNAM), Mexico, Mexico
e-mail: pandiyan@unam.mx

synthesis and applications of imidazole-based Pd complex in Heck reaction [27]. Here, we extended the application of such ligands in the synthesis of Au(I) complexes. In this study, the design and synthesis of several imidazole-based NHC–Au(I) complexes are reported (Scheme 1). NHC–Au(I)-modified electrodes are investigated in the electrocatalytic oxidation of glucose. This method is applied directly for the clinical determination of glucose. To the best of our knowledge, there is no report for the glucose oxidation at NHC–Au(I)-modified electrodes.

2 Experimental details

2.1 Materials

All chemicals used for the synthesis of complex were of A.R. Grade and purchased from Aldrich and used as received without further purification. H_2SO_4, NaOH, D-(+)-glucose, L-ascorbic acid, and uric acid were obtained from Merck India Pvt. Ltd. Nafion (5 %, v/v) was purchased from Aldrich. The electrochemical measurements were performed in 0.1 M NaOH solution. Deionized water from Millipore Milli-Q system (Resistivity 18.2 MΩ cm) was used in the electrochemical studies. Blood serum samples were obtained from Parmar Hospital, Ropar, Punjab, India.

2.2 Characterization

Nuclear magnetic resonance (NMR) spectra were recorded on Varian Inova-300 MHz NMR. Elemental analysis was carried out on a Fisons (Model EA 1108 CHNSO). Mass Spectrometer (FAB-MS) (Model Thermo-Electron) equipped with Double Focus Sector was used to analyze the mass fragments of the compounds.

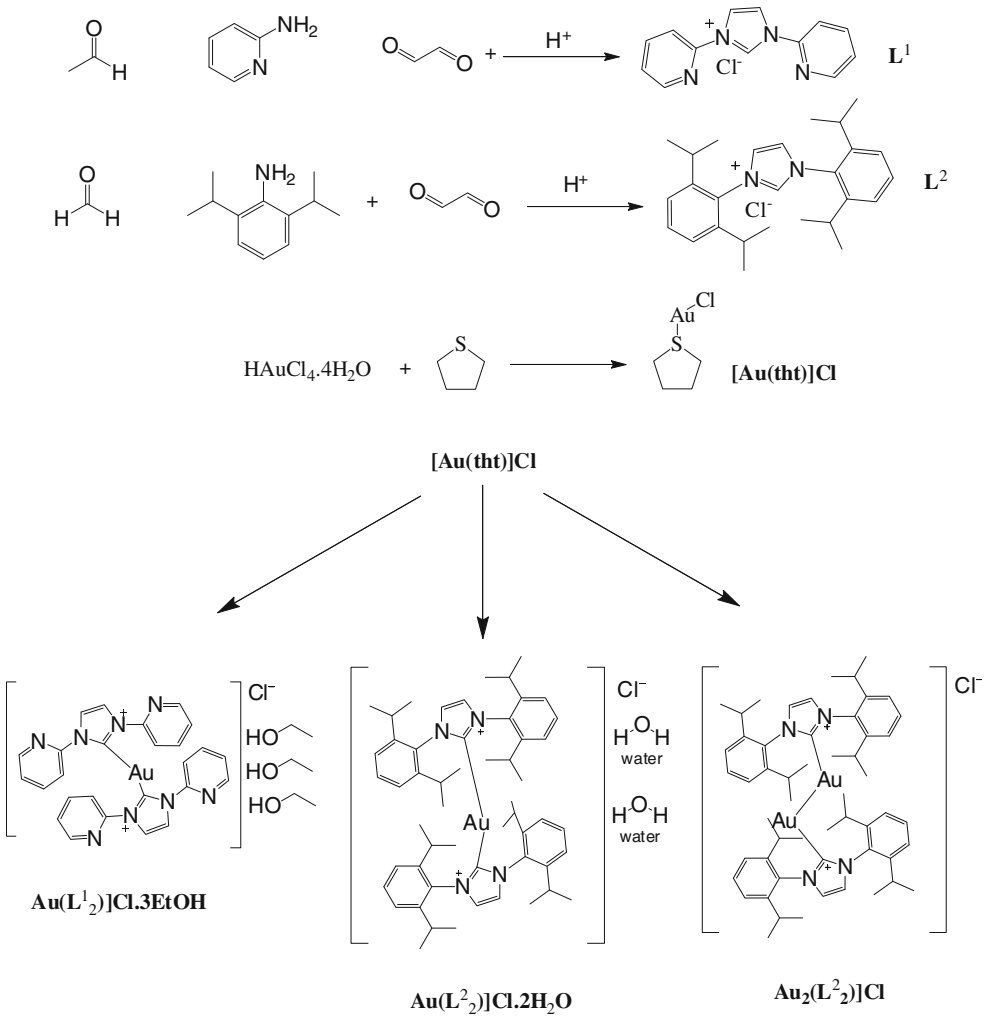

Scheme 1 Schematic representations for the synthesis of ligands and NHC–Au(I) complexes investigated in this study

2.3 Synthesis of Au(I) complexes

2.3.1 Preparation of 1,3-bis(aminopyridyl-2-yl)imidazolium chloride (L^1)

Ligand L^1 was prepared following the reported procedure [28]. To a stirred solution of 2-aminopyridine (10.0 mmol) in MeOH (40.0 mL), aqueous glyoxal (5.0 mmol) and paraformaldehyde (5.0 mmol) were added, followed by the drop wise addition of HCl (5.0 mmol). The resulting mixture was refluxed for 36 h with stirring, and then it was cooled to room temperature. The brown oil compound was obtained by evaporating the solvent in a rotary evaporator. The compound was re-crystallized by dissolving with a minimum amount of methanol and ether solvent (yield, 53.0 %).

Elemental analysis for $C_{13}H_{11}N_4Cl$ Calcd.: C, 60.34; H 4.25; N 21.66. Found: C, 60.45; H, 4.29; N, 21.76. ^{1}H NMR (300 MHz, CD_3OD) δ (ppm): 6.89–8.21 (m, 8H, pyridyl; s, 2H, –N–CH=CH–N–, imidazole), 8.73 (s, 1H, –N–CH=N–, imidazole).

2.3.2 Preparation of 1,3-bis(2,6-diisopropylphenyl)imidazolium chloride (L^2)

Ligand L^2 was prepared following the reported procedure [29]. A mixture of glyoxal (5.0 mmol) and formaldehyde (5.0 mmol) were added to a solution of 2,6-diisopropylphenylamine (10.0 mmol) and methanol (40.0 mL), followed by the drop wise addition of HCl (5.0 mmol). The reaction mixture was refluxed for 36 h, and then it was cooled to room temperature. An oily compound was obtained by evaporating the solvent in a rotary evaporator. The compound was re-crystallized by dissolving with a minimum amount of methanol and ether solvent (yield, 84.6 %).

Elemental analysis for $C_{27}H_{37}N_2Cl$: Calcd.: C, 76.32; H, 8.71; N, 6.59. Found: C, 75.30; H, 8.49; N, 6.79. ^{1}H NMR (300 MHz, CD_3OD) δ (ppm): 1.29 (d, 24H, CH_3–, isopropyl), 2.84 (m, 4H, (CH–, isopropyl), 7.52–7.69 (m, 6H, Ar–H), 8.39 (s, 2H, –N–CH=CH–N, imidazole ring), 10.07 (s, 1H, –N–CH=N–, imidazole ring).

2.3.3 Preparation of chloro(tetrahydrothiophene) gold(I) [Au(tht)]Cl

[Au(tht)]Cl was prepared by following the reported procedure [30]. $HAuCl_4$ (15 mmol) and tetrahydrothiophene (30.0 mmol) were added slowly to a 50 mL solution of water and ethanol (water:ethanol, 1:5) with stirring in dark condition. During the reaction, a yellow precipitate was initially formed, which was transformed to colorless solid after 30 min. Compound was filtered, washed with 30 mL of ethanol, and dried in the vacuum.

2.3.4 Preparation of the gold complexes ($[Au(L^1{}_2)]Cl\bullet 3EtOH$, $[Au(L^2{}_2)]Cl\bullet 2H_2O$ and $[Au_2(L^2{}_2)]Cl$

Gold complexes were made by following the reported procedure but with little modification [28, 31–33]. Ligand (L^1 or L^2: 1.5 mmol) dissolved in CH_2Cl_2 (20.0 mL) was added slowly to a solution of [Au(tht)]Cl (0.75 mmol) in CH_2Cl_2 (10.0 mL). The resulting solution was stirred for 25 min at 308 K in the absence of light. Reaction mixture was filtered through aluminum oxide. An oily product was obtained after the evaporation by a rotary evaporator. Products were re-crystallized with the solvent mixture of acetonitrile/ethanol and were finally washed with ether to afford white crystalline compounds ($[Au(L^1{}_2)]Cl\bullet 3EtOH$ (Yield, 76.4 %) and $[Au(L^2{}_2)]Cl\bullet 2H_2O$ (Yield, 89.3 %)).

For the synthesis of $[Au_2(L^2{}_2)]Cl$, [Au(tht)]Cl (1.5 mmol) was taken in CH_2Cl_2 (20.0 mL), rest all the procedure was the same as discussed above for the synthesis of $[Au(L^1{}_2)]$-$Cl\bullet 3EtOH$/$[Au(L^2{}_2)]Cl\bullet 2H_2O$ (yield, 86.2 %).

Elemental analysis for $[Au(L^1{}_2)]Cl\bullet 3EtOH$; ($[C_{26}H_{20}N_8Au]Cl\cdot 3CH_3CH_2OH$); Calcd.: C, 47.15; H, 4.70; N, 13.75. Found: C, 47.90; H, 4.35; N, 14.96. FAB-MS (*m*/*z* %): 815 $[M^+, C_{32}H_{38}AuClN_8O_3]^+$, 663 (6.0 %) $[C_{26}H_{26}AuN_8O]^+$, 309 (12.0 %) $[C_4H_8AuN_4]^+$, 153 (100 %) $[C_7H_{13}N_4]^+$, 136 (90.0 %) $[C_6H_9N_4]^+$, 107 (54.0 %) $[C_6H_7N_2]^+$, 57 (66.0 %) $[C_3H_7N]^+$ (Figs. S1, S2 of SI). ^{1}H NMR (300 MHz, acetone-d_6) δ (ppm) = 6.88–8.36 (m, 16H, pyridyl; s, 4H, imidazole) (Fig. S3 of SI).

Elemental analysis for $[Au(L^2{}_2)]Cl\bullet 2H_2O$; ($[C_{54}H_{72}N_4Au]Cl\cdot 2H_2O$); Calcd.: C, 62.03; H, 7.33; N, 5.36. Found: C, 60.95; H, 6.41; N, 5.23. FAB-MS (*m*/*z* %): 1042 $[M^{2+}, C_{54}H_{76}AuClN_4O_2]^{2+}$, 389 (100 %) $[C_{27}H_{36}N_2]^+$, 186 (10.0 %) $[C_{12}H_{14}N_2]^+$, 91 (3.0 %) $[C_6H_5N]^+$ (Figs. S4, S5 of SI). ^{1}H NMR (Varian 300 MHz, acetone-d_6) δ (ppm) = 1.32 (d, 48H, isopropyl), 2.86 (c, 8H, isopropyl), 7.51–7.66 (m, 12H, benzene ring), 8.24 (s, 4H, imidazole) (Fig. S6 of SI).

Elemental analysis for $[Au_2(L^2{}_2)]Cl$, ($[C_{54}H_{72}N_4Au]Cl$): Calcd.: C, 53.42; H, 5.84; N, 4.70. Found: C, 50.43; H, 5.09; N, 4.17. FAB-MS (*m*/*z* %): 1192 $[M^+, C_{54}H_{71}N_4Au_2Cl]^+$, 299 (53.0 %) $[C_{20}H_{30}N_2]^+$, 228 (25.0 %) $[C_{15}H_{21}N_2]^+$, 154 (85.0 %) $[C_9H_{18}N_2]^+$, 137 (100 %) $[C_9H_{15}N]^+$, 77 (38.0 %) $[C_6H_5]^+$ (Figs. S7, S8 of SI). ^{1}H NMR (300 MHz, acetone-d_6) δ (ppm) = 1.31 (d, 48H, isopropyl), 2.86 (c, 8H, isopropyl), 7.49–7.64 (m, 12H, benzene ring), 8.24 (s, 4H, imidazole) (Fig. S9 of SI).

2.4 Fabrication of modified electrodes

Cyclic voltammetry (CV) and amperometric studies of Au(I) complexes were performed using Potentiostat–Galvanostat BASi EPSILON, USA. A three-electrode

electrochemical cell was employed with Ag/AgCl as the reference electrode (3 M KCl), Au(I) complexes were mounted on glassy carbon (GC) (3 mm diameter) as the working electrode, and Pt foil as the counter electrode. Before modification, the electrode was ultra-sonicated in ethanol and deionized water for 5 min, respectively. 10 μL aliquot of NHC–Au(I) suspension (a homogenous sonicated solution of 5 mg of Au(I) complex and a mixture of 0.1 mL of Nafion and 0.9 mL of distilled water) was placed onto the electrode surface, the electrode was dried in air, leaving the material mounted onto the GC surface.

2.5 Clinical method for the determination of glucose in blood serum

Blood was collected in heparinized vials. Whole blood obtained (directly from patients) was allowed to clot for 1 h and serum was separated and used for analysis. Glucose oxidase–peroxidase (GOD–POD) was used as a reagent in the hospital for the quantitative determination of glucose in serum. The method selectively estimates β-D-glucose in serum. One reagent blank and one standard are required for the analysis. 10 μL blood serum and 1 mL of GOD–POD solution were mixed well and incubated for 15 min at 310 K. Absorbance of standard and sample against a blank reagent was measured at 505 nm using Biochemistry analyzer microlab 300, Merck. Glucose concentration in the serum was calculated by using the following formula:

$$\text{Glucose}\,(\text{mg dL}^{-1}) = \text{Absorbance of sample} \times \text{conc. of std.}\,(\text{mg dL}^{-1})/\text{absorbance of standard.}$$

3 Results and discussion

3.1 Synthesis and computational study of Au complexes

For the synthesis of Au complexes ([Au(L^1_2)]Cl•3EtOH, [Au(L^2_2)]Cl•2H_2O, and [Au_2(L^2_2)]Cl, first ligands, L^1 and L^2, were prepared by the multistep synthesis route. Ligands were then reacted with the gold precursor [Au(tht)]Cl, which was synthesized by the reaction of $HAuCl_4$ and tetrahydrothiophene (Scheme 1). Complexes were characterized by various spectroscopic tools (details are provided in the "Experimental details" section and Supplementary Information section).

Structures of ligands and Au complexes synthesized in this study were theoretically computed using Gaussian 09 Software. Geometry of ligands was optimized using DFT/B3LYP/unrestricted spin method with LANL2DZ basis set (Figs. S10, S11; Table S1 of supporting information (SI)). Molecular energy orbitals calculated using DFT show that the difference in the energy between HOMO and LUMO for L^2 is somewhat higher than L^1. For the complexes, all calculations were performed with DFT/B3LYP/unrestricted method, and with the LANL2DZ method due to the broad capacity of this basis set to work with heavy atoms like gold. Optimized structures of complexes are shown in Figs. 1, 2, and 3 and theoretical parameters are provided in Tables S2 and S3 of SI.

Even though all three complexes were expected to be symmetric, however, a small difference in bond lengths was observed in theoretical data. This could be explained through the mechanism of formation of the complex. L^1 gets attached to the gold atoms without any interference and form the carbon–gold bond easily. When L^2 forms bond with the gold atom, a change in the conformation in the ligand was observed to avoid the electrostatic interference with all the atoms from the ligand. Only a marginal energy difference of the molecular orbital energies for all complexes was observed. This is due to the stabilization provided by a big gold atom to the complexes. [Au_2(L^2_2)]Cl has the lowest energy gap between the HOMO and HOMO-1 molecular orbitals (0.018 Hf; 0.489 eV) (Table S3 of SI), this could lead to the highest reactivity, because both orbitals can be involved in the reaction.

Conductivity of NHC–Au(I) complexes were investigated. For the conductivity measurements, sample (0.1 g) was pelletized using IR pellet maker and contact points were made using silver paste. The conductivities of the pellet of NHC–Au(I) complexes were measured at room temperature (see Table 1). Conductivity of [Au_2(L^2_2)]Cl was found to be the highest among all the NHC–Au(I) complexes samples investigated in this study.

3.2 Electrochemical oxidation of glucose using Au complexes

For electrochemical oxidation, [Au(L^1_2)]Cl•3EtOH, [Au(L^2_2)]Cl•2H_2O, and [Au_2(L^2_2)]Cl modified electrodes, represented as [Au(L^1_2)], [Au(L^2_2)], and [Au_2(L^2_2)], respectively, were fabricated. To investigate the electrocatalytic behavior of the modified electrodes, the CV of [Au(L^1_2)] modified electrode was measured in a 0.1 M H_2SO_4 at 50 mV s^{-1} (Fig. 4). The voltammetric curve of [Au(L^1_2)]-modified electrode measured in 0.1 M H_2SO_4 demonstrated oxidation in the positive scan (1.1 V) and reduction on the negative scan (0.65 V) [34–37]. The voltammogram of gold in the alkaline medium (0.1 M NaOH) is similar to that of a bulk gold electrode (Fig. 5). The anodic peak i is due to the anodic discharge of water, with the formation of a sub monolayer of adsorbed hydroxyl radicals [38, 39], while the oxidation wave (ii) is associated with Au(III) formation. The cathodic peaks iii and iv in the negative sweep are associated to the reduction of Au(III) species.

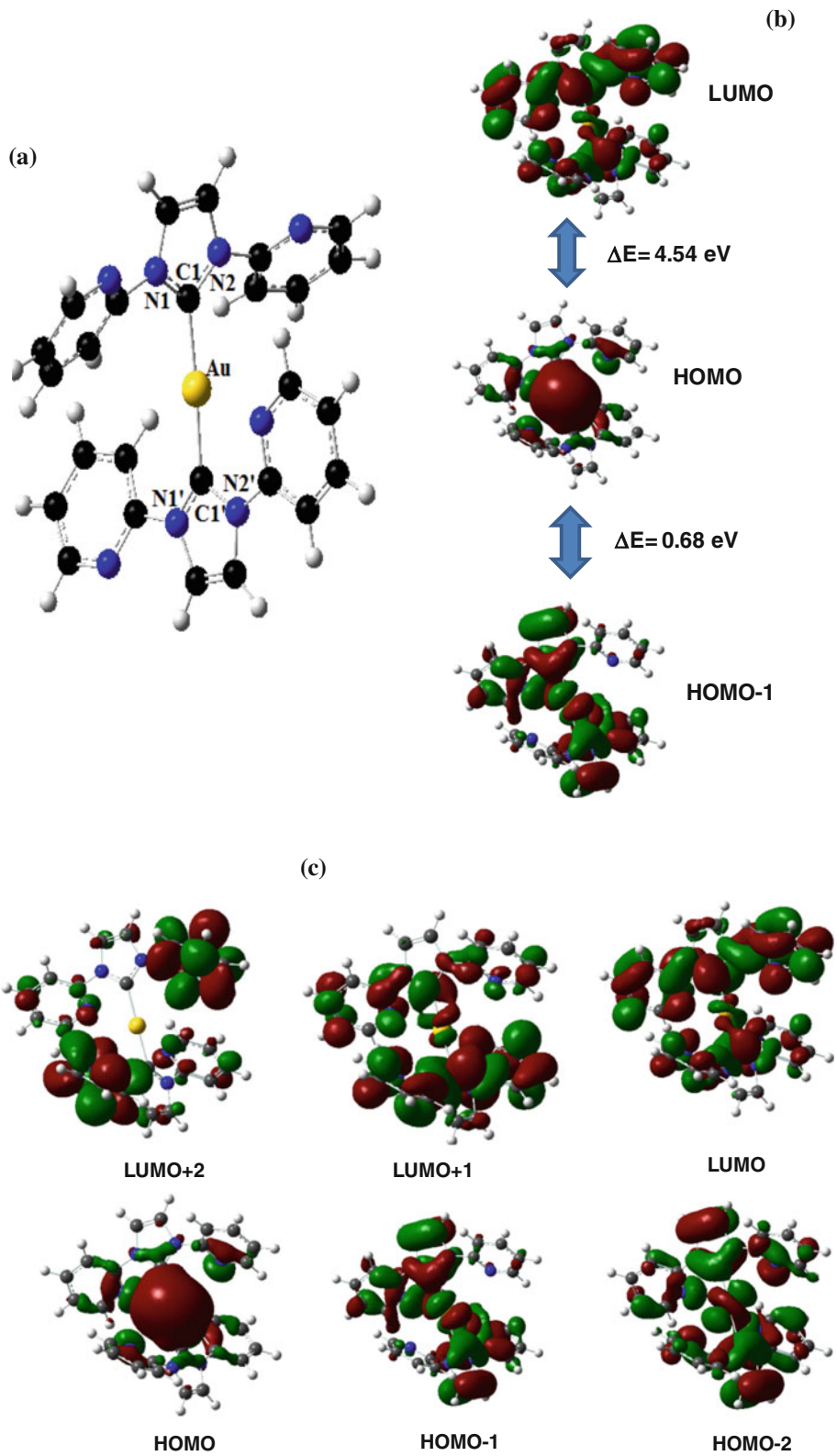

Fig. 1 **a** Optimized structure, **b** molecular orbital energy diagram, and **c** main molecular orbitals diagram of [Au(L^1_2)]

Voltammetric method was used to investigate and compare the catalytic activities of the NHC–Au(I)-modified electrodes for the non-enzymatic detection of glucose in the alkaline medium. CV for NHC–Au(I)-modified electrodes represent a typical two-step oxidation process in the positive scan of potential, in which two oxidation peaks are observed (Fig. 6). The first oxidation peak at around −0.40 V (anodic peak i) is attributed to the

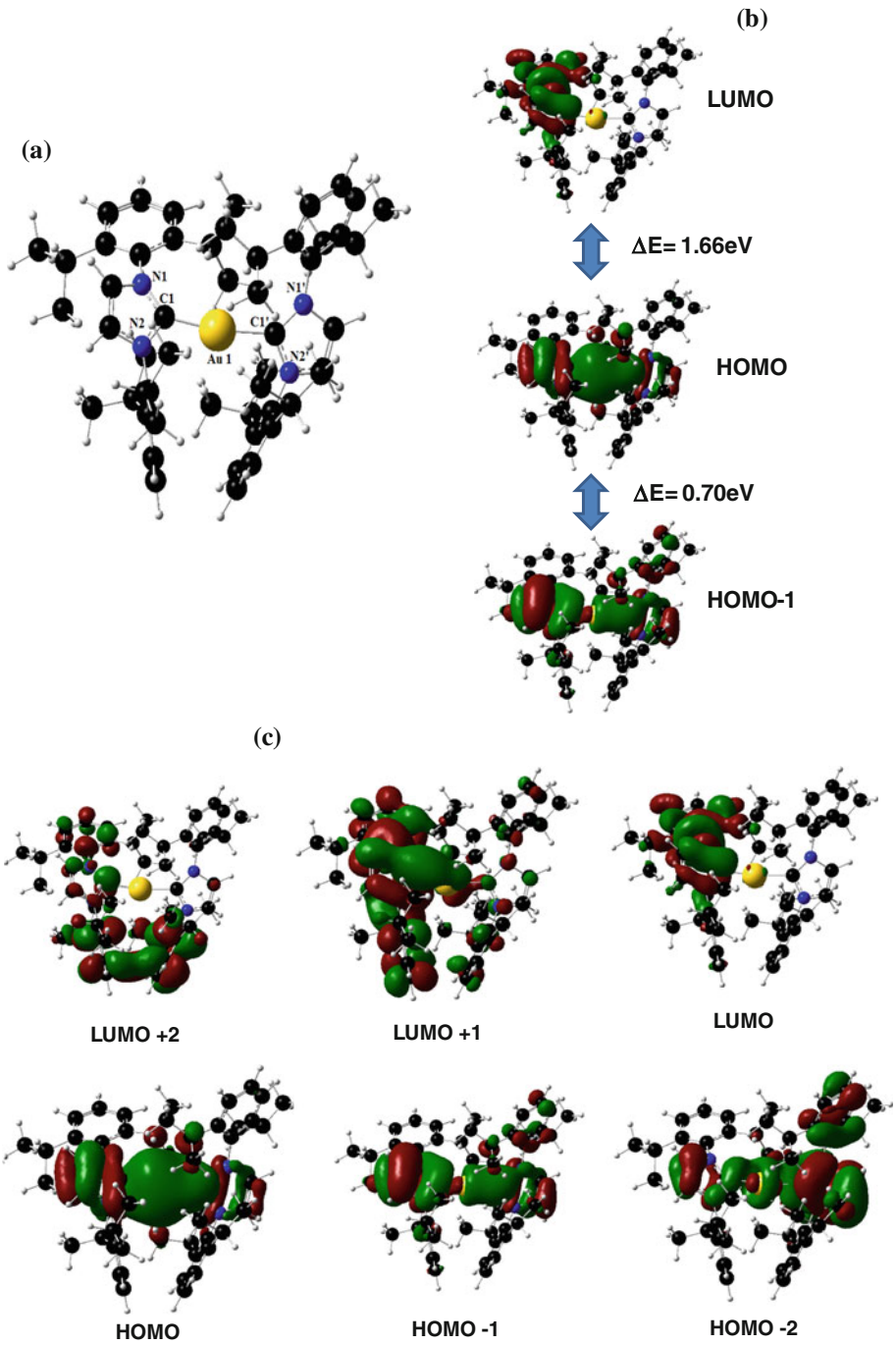

Fig. 2 **a** Optimized structure, **b** molecular orbital energy diagram, and **c** main molecular orbitals diagram of orbital energy diagram of [Au(L^2_2)]

oxidation of glucose to gluconolactone [40], while the second anodic oxidation peak ii centered at 0.25 V, corresponds to the subsequent oxidation of gluconolactone [41]. It is generally accepted that gold hydroxide species acts as the active species for glucose oxidation, therefore, the oxidation of glucose is strongly dependent on the number of gold hydroxide sites. At around −0.40 V, there are very limited numbers of gold hydroxide sites within the Au complex. When the potential positively shifts to 0.25 V, the population of the gold hydroxide sites on the electrode surface increases and subsequent oxidation of gluconolactone takes place (Scheme 2) [41]. A further positive shift in the potential at around 0.50 V gives rise to the formation of gold(III) species, which leads to a decrease in the density of the gold hydroxide sites and suppresses the electrocatalytic oxidation of glucose and its derivatives. Among the NHC–Au(I)-modified electrodes, such phenomenon was observed for [Au(L^2_2)]-modified electrode, as a result, the current in the CV curves decreases (Fig. 6b). On the other hand, the negative potential scan shows that a reduction in the Au(III) occurs and Au(I) hydroxide active sites re-form. Thus, enough

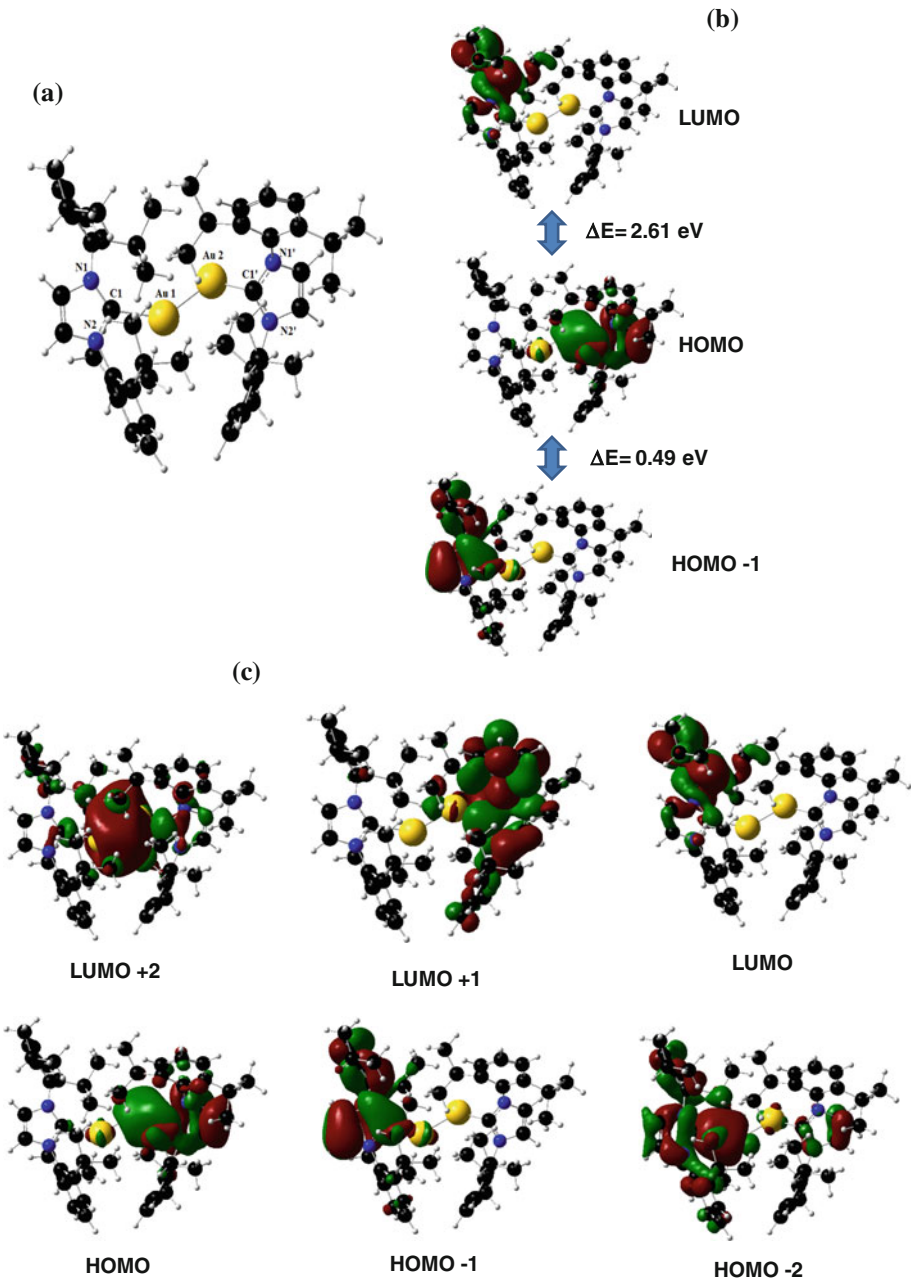

Fig. 3 **a** Optimized structure, **b** molecular orbital energy diagram, and **c** main molecular orbitals diagram of $[Au_2(L^2{}_2)]$

Table 1 Conductivity of NHC–Au(I) complexes synthesized in this study

Samples	Conductivity (S cm^{-1})
$[Au(L^1{}_2)]Cl.3EtOH$	0.048
$[Au(L^2{}_2)]Cl.2H_2O$	0.036
$[Au_2(L^2{}_2)]Cl$	0.074

active sites are available for the direct oxidation of glucose, resulting in the appearance of oxidation peak during cathodic direction of the potential sweep at 0.07 V (iii) [41]. Au(I) complexes investigated in this study show different electrocatalytic activity toward glucose oxidation. Among the NHC–Au(I) complexes investigated, $[Au_2(L^2{}_2)]$ exhibited the highest current (Fig. 6c), which signifies its high electrocatalytic activity. Overall one can conclude that Au(I) complex at the modified electrode surface undergoes pre-monolayer oxidation to form hydrous Au(I) species at a lower potential (−0.4 V) and Au(III) hydrous species at a higher potential (0.25 V). The oxidation of glucose in alkaline media is mainly mediated by the Au(III) hydrous species at a higher potential (0.25 V in the present result) and a combination of Au(I) and Au(III) hydrous species at the potential below 0.1 V (Scheme 2).

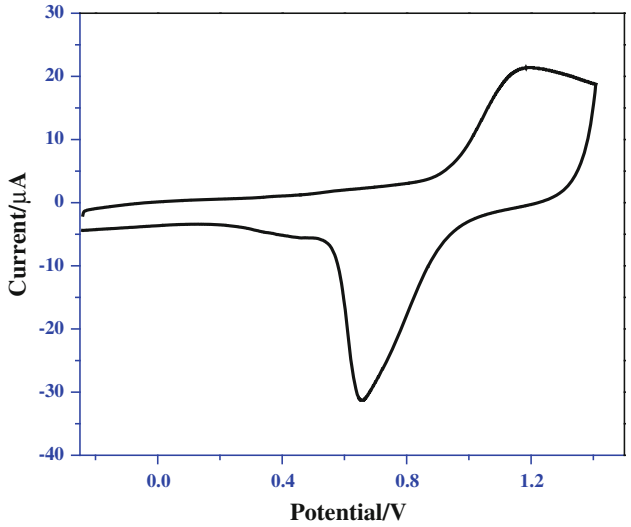

Fig. 4 The CV of $[Au(L^1_2)]$-modified electrode in 0.1 M H_2SO_4 at a scan rate of 50 mV s^{-1}

3.3 Effect of scan rate

In order to study the rate-determining step of the glucose oxidation using $[Au_2(L^2_2)]$-modified electrodes, CV was recorded at a fixed molar concentration of glucose (3 mM) by varying scan rates (v) (Fig. 7). It was observed that by varying the scan rate, the current density of various peaks (i, ii, and iii) varies. The variations in the peak current as a function of $v^{1/2}$ for peaks i, ii, and iii are shown (Fig. 7, inset). Peak currents found to vary linearly with $v^{1/2}$ for peak ii, suggesting that electrochemical reaction occurring at this potential (peak ii) is a diffusion-controlled process [42]. The result is in good agreement with the proposed mechanism for peak ii [41], in which the gold hydroxide species favors direct oxidation of glucose.

Glucose sensing was investigated using CV and continuous amperometry at NHC–Au(I)-modified electrodes. First CV was taken on the successive addition of glucose (Figs. 8, S12, S13 of SI). The CV of glucose at bare Au electrode sensed glucose up to 4 mM with low current when compared to NHC-modified electrodes (Fig. S14 of SI). All NHC–Au(I)-modified electrodes show similar sensing ability, however, the current response for $[Au_2(L^2_2)]$ was found to be the best among the NHC–Au(I) complexes investigated in this study (Figs. 8, S12, S13 of SI). The highest activity of $[Au_2(L^2_2)]$-modified electrode toward glucose oxidation is due to the highest conductivity of $[Au_2(L^2_2)]$ compared to other NHC–Au(I) complexes investigated in this study.

3.4 Dependence of the response current on the applied potential

To find the optimal conditions for the amperometric sensing of glucose, the effect of applied potential on the response current of the sensor was investigated. Amperometric response at $[Au_2(L^2_2)]$-modified electrode in 0.1 M NaOH solution on successive addition of 2 mM glucose at different applied potentials (ranging from −0.4 to 0.45 V) was measured (Fig. S15 of SI). In the range of +0.1 to +0.4 V, the oxidation current of glucose increased by increasing potential. The maximum response current with a

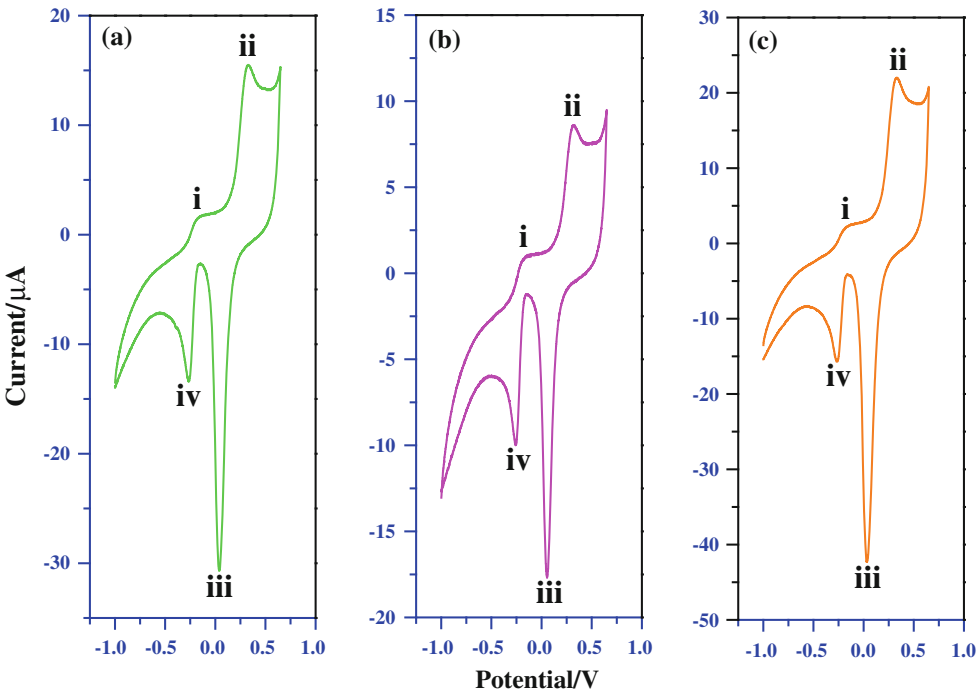

Fig. 5 CV of the **a** $[Au(L^1_2)]$, **b** $[Au(L^2_2)]$, and **c** $[Au_2(L^2_2)]$-modified electrodes in a 0.1 M NaOH solution at a scan rate of 50 mV s^{-1}

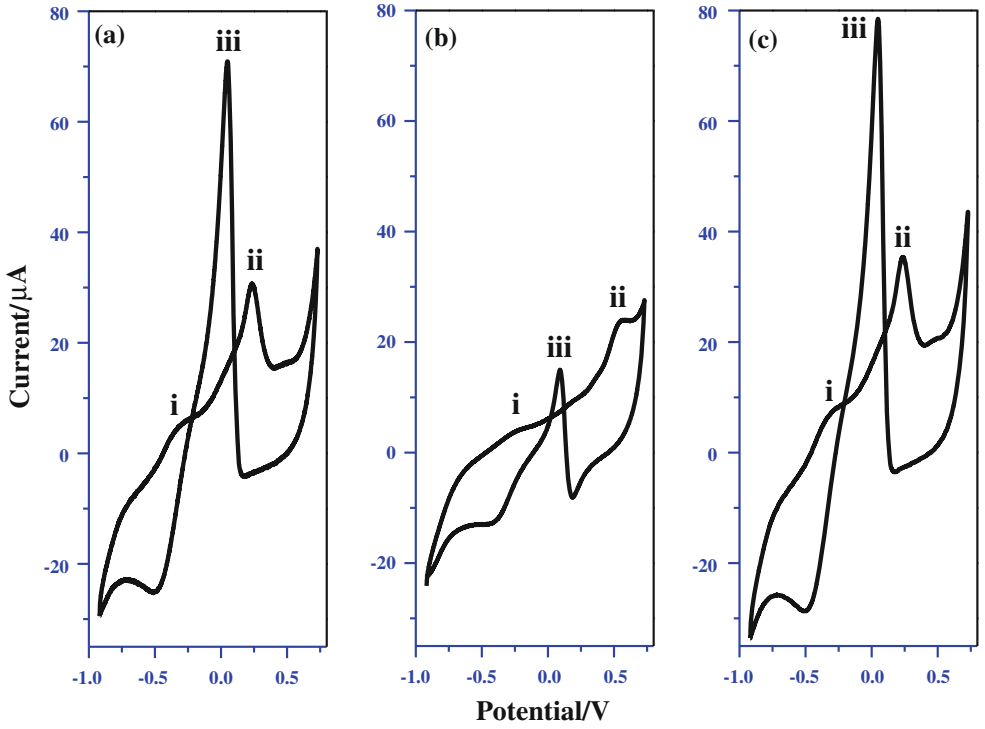

Fig. 6 CV of the **a** [Au(L^1_2)], **b** [Au(L^2_2)], **c** [Au_2(L^2_2)]-modified electrodes in a 0.1 M NaOH solution of 16 mM glucose at a scan rate of 50 mV s^{-1}

Scheme 2 Oxidation mechanism of glucose at NHC-modified electrode

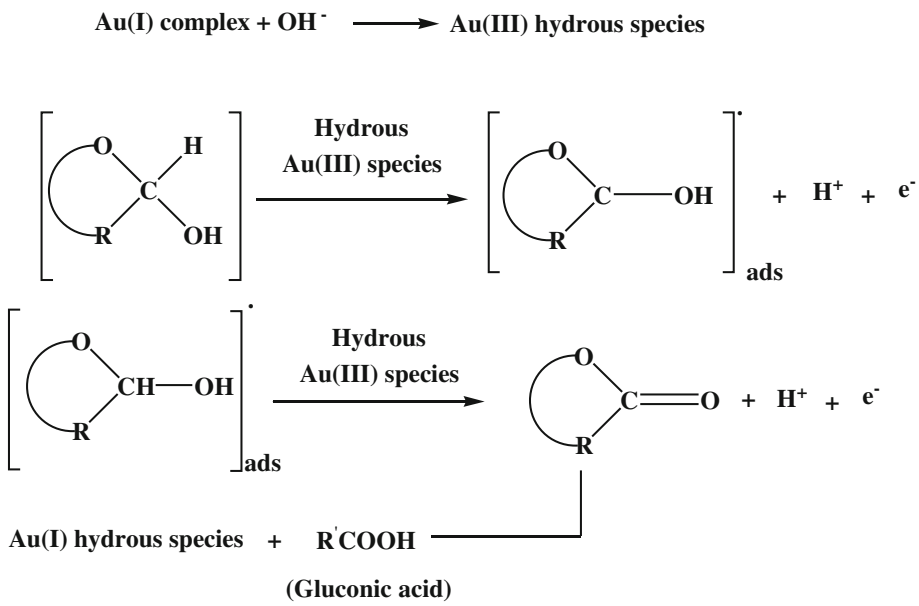

good signal/noise ratio was achieved at +0.4 V. Thus, a constant potential of +0.4 V was chosen for further amperometric investigations.

3.5 Amperometric responses to glucose concentration

For continuous amperometry studies, aliquots of glucose were successively added into 10 mL NaOH solution (0.1 M) at applied potentials of +0.40 V (Fig. 9a). The amperometric current obtained is proportional to the concentration of glucose in the reaction vessel. The addition of glucose is marked by arrows at the concentrations mentioned. The value of the current was plotted against the concentration of glucose to obtain a calibration plot (Fig. 9a, inset). The sensor exhibits excellent linearity in the range of 10 μM–20 mM with linear regression 0.99

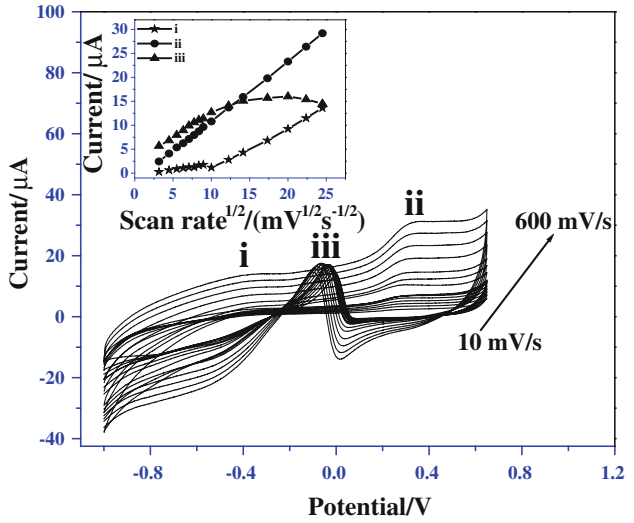

Fig. 7 CV responses of $[Au_2(L^2_2)]$-modified electrodes with 1 mM glucose at various scan rates from 10 to 600 mV s^{-1} in 0.1 M NaOH solution. *Inset* shows the plot of the oxidation peak currents against the square root of scan rates

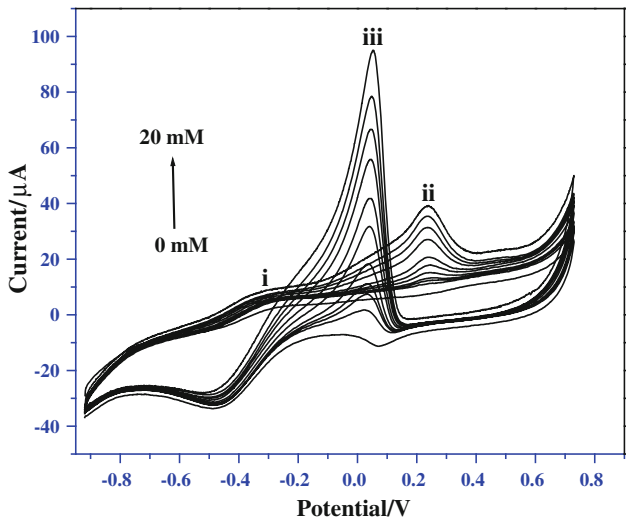

Fig. 8 CV responses of the $[Au_2(L^2_2)]$-modified electrode in the presence of glucose in 0.1 M NaOH at a scan rate of 50 mV s^{-1}

and limit of detection (LOD) of 2.9 μM. Calibration curve of $[Au(L^1_2)]$ and $[Au(L^2_2)]$-modified electrode exhibits a linear response up to 16 mM, but with low current sensitivity compared to $[Au_2(L^2_2)]$-modified electrode (Figs. S16, S17 of SI). Theoretical calculation shows that the Au–C bond length is almost similar (≈2.06 Å) in $[Au(L^1_2)]$, but they were found to be different (1.95 and 2.08 Å) in $[Au(L^2_2)]$. Short bond length in $[Au(L^2_2)]$ may be one of the reasons for the low activity of $[Au(L^2_2)]$ compared to $[Au(L^1_2)]$. Geometrical optimized structure confirms that due to the steric hindrance, change in the conformation in the ligand takes place to avoid the electrostatic interference with all the atoms. Due to this

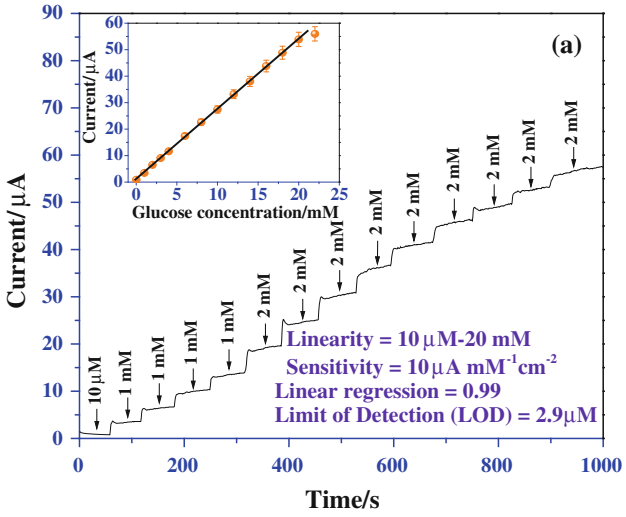

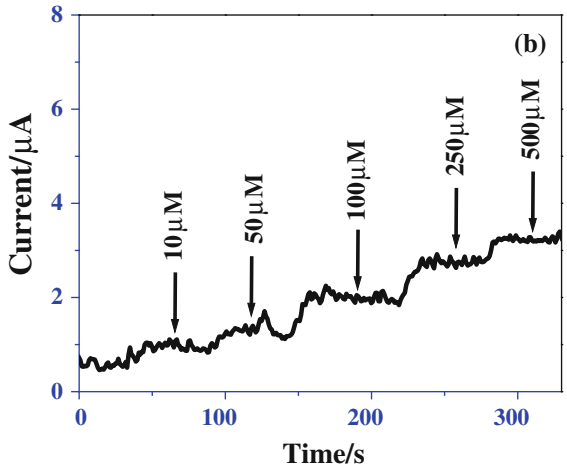

Fig. 9 **a** Amperometric responses of the $[Au_2(L^2_2)]$-modified electrode to the successive addition of glucose at applied potential of +0.4 V. *Inset* shows the calibration curve for the sensor response to glucose. **b** Current–time response curve of the sensor upon successive additions of 10, 50, 100, 250, and 500 μM glucose

conformational change, accessibility of glucose molecules to the Au active site is restricted; therefore, the activity of $[Au(L^2_2)]$ was found to be less compared to $[Au(L^1_2)]$. High activity of $[Au_2(L^2_2)]$ is due to the presence of Au–Au bond in $[Au_2(L^2_2)]$ when compared to $[Au(L^2_2)]$, which promotes the accessibility of the reactant molecules to the Au active sites due to less steric hindrance. The Au–C bond lengths were found to more in $[Au_2(L^2_2)]$ when compared with $[Au(L^2_2)]$ (Table S2 of SI) that may also enhance accessibility of the reactant molecules to the Au active sites and promote its activity. The high reactivity of $[Au_2(L^2_2)]$ can also be correlated with the lowest energy gap between the HOMO and HOMO-1 molecular orbitals, because both orbitals can be involved in the reaction. As shown in Table 2, most of the analytical properties corresponding to $[Au_2(L^2_2)]$-modified electrode are comparable or even

Table 2 Comparison of some non-enzymatic glucose sensors in terms of LOD, linear range, and sensitivity

Electrode materials	LOD (μM)	Linear range (mM)	Sensitivity (μA mM^{-1} cm^{-2})	References
Pt–Au/MWCNT	10	0.04–24.4	10.7	[10]
Pt–Pd NWAs	8.0	1–11	11.2	[11]
Pt NTAEs	1.0	2–14	0.1	[12]
PtM (M = Ru, Pd, and Au)	50	Up to 15	10.6	[15]
UGSs	10	0.2–13.2	16.8	[35]
$[Au_2(L^2_2)]$	2.9	0.01–20	10	This work

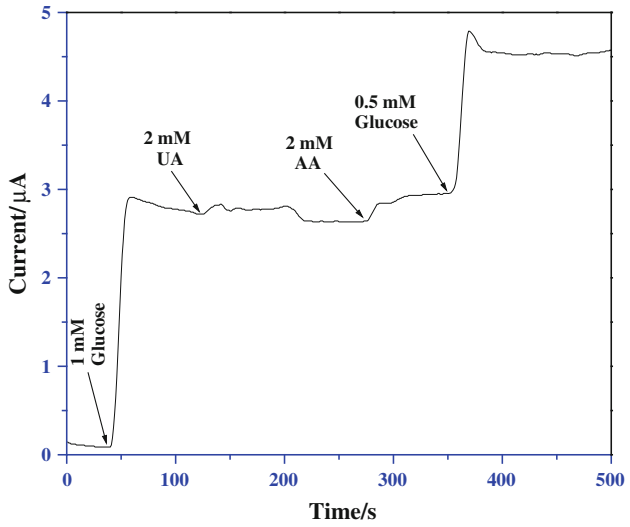

Fig. 10 Current responses of $[Au_2(L^2_2)]$-modified electrode to the sequential additions of 1 mM glucose, 2 mM UA, 2 mM AA, and 0.5 mM glucose at +0.4 V

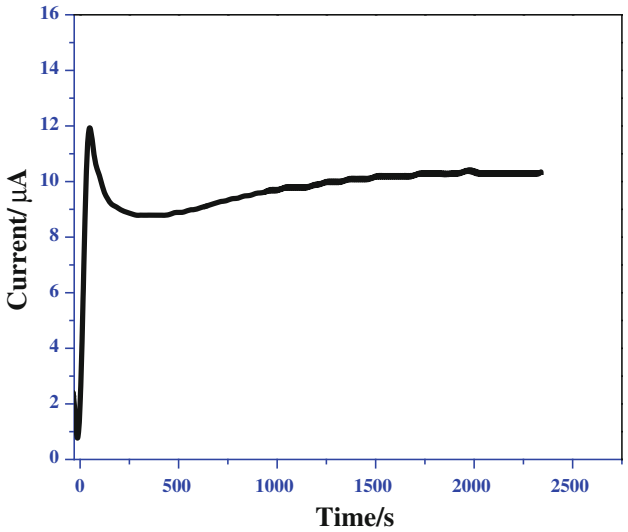

Fig. 11 The response stability of $[Au_2(L^2_2)]$-modified electrode to the addition of 170 mg dL^{-1} serum sample at applied potential of 0.4 V

better than the results reported in the literature [10–12, 15, 41, 42].

3.6 Selectivity aspects, reproducibility, and stability

The selectivity of the method was evaluated by testing the response of $[Au_2(L^2_2)]$-modified electrode toward several species that coexist in blood along with glucose, such as ascorbic acid (AA), and uric acid (UA) (Fig. 10). It may be noted that the normal concentration ranges of AA and UA in the human blood are 34–79 and 180–420 μM, respectively [43]. The response current for these interfering species (even at this high concentration) is less than 4 % than that of glucose at +0.4 V. Interference from other saccharides, such as fructose, mannose, and lactose was also investigated. Interference tests were carried out by mixing the sugars (200 μM mannose or 200 μM lactose or 6,000 μM of fructose) that could potentially interfere with the glucose (2 mM) detection. The sugar concentrations selected for these tests were based on their physiologically significant values reported in the literature. For example, serum fructose concentration in patients with diabetes was reported to be around 12.0 ± 3.8 μM [44]. The glucose measurements obtained from these mixtures were compared with the measurements made from glucose alone. Only a marginal shift in response current (+1.1, −0.9, and +0.5 % for fructose, lactose, and mannose, respectively) was observed in the presence of these interfering sugars. This result encouraged us to investigate $[Au_2(L^2_2)]$-modified electrode for the detection of glucose in blood serum. The long-term stability of the sensor was evaluated by measuring its sensitivity for 21 days using 1.0 mM glucose. The sensor was stored in air at ambient conditions, and its sensitivity was measured at the interval of every 3 days. The CV response of the electrode to 1.0 mM glucose decreased less than 3.5 %, which indicates that the electrode has good reproducibility and excellent stability. The reproducibility and repeatability of the sensor were evaluated in glucose sensing studies. Five different $[Au_2(L^2_2)]$-modified electrodes were fabricated under identical condition and investigated toward 2.0 mM glucose. Three measurements were taken for each electrode. The relative standard deviation (RSD) was found to be 2.4 %, indicating a high inter-electrode reproducibility. To

Table 3 Determination of glucose in the human blood serum samples

Samples	Determined by hospital	Measured by $[Au_2(L^2_2)]$-modified electrode	RSD (%)
1	189.5 mg dL^{-1}/4.9 mM L^{-1}	181.7 mg dL^{-1}/4.7 mM L^{-1}	4.2
2	170.1 mg dL^{-1}/4.4 mM L^{-1}	174.8 mg dL^{-1}/4.5 mM L^{-1}	2.6
3	205.7 mg dL^{-1}/5.3 mM L^{-1}	201.5 mg dL^{-1}/5.2 mM L^{-1}	2.1
4	150.8 mg dL^{-1}/3.9 mM L^{-1}	143.0 mg dL^{-1}/3.7 mM L^{-1}	5.4
5	176.3 mg dL^{-1}/4.6 mM L^{-1}	178.7 mg dL^{-1}/4.6 mM L^{-1}	1.2

show the repeatability, $[Au_2(L^2_2)]$-modified electrode was used continuously for a series of ten voltammetry tests toward 2.0 mM glucose, giving a RSD of 4.3 %.

3.7 Real sample analysis

Human serum samples were analyzed in 0.1 M NaOH solution to demonstrate the practical application of $[Au_2(L^2_2)]$-modified electrode [45–47]. Five different human blood serum samples were investigated. The blood glucose concentration was calculated from the calibration curve. The obtained results were satisfactory and comparable with the clinical results (Table 3).

Amperometry was used to evaluate the antifouling property of the $[Au_2(L^2_2)]$-modified electrode using 170 mg dL^{-1} serum sample. The response of the $[Au_2(L^2_2)]$-modified electrode remained stable during 40 min at +0.4 V, with only less current diminutions for the oxidation of glucose (Fig. 11). The result demonstrates that favorable antifouling property can be achieved at $[Au_2(L^2_2)]$-modified electrode, which prevented the electrode from passivation.

4 Conclusions

All NHC–Au(I) complexes investigated in this study were found to be active for the electrocatalytic oxidation of glucose. Electrocatalytic activity of $[Au_2(L^2_2)]Cl$ was found to be the best among the NHC–Au(I) complexes investigated in this study. Conductivity measurements and DFT calculation explained the reason for the high activity of $[Au_2(L^2_2)]Cl$. The sensor exhibited excellent reproducibility, repeatability, antifouling, and anti-interference characteristics in the blood serum analysis. Applicability of NHC–Au(I)-based non-enzymatic sensors can be extended to other electroactive species found in blood serum, food, and pharmaceutical products.

Acknowledgments This work was supported by Indo-Mexican Joint Research Project [DST/INT/MEX/01-04/2011(iii)]. AP is grateful to CSIR, New Delhi for SRF fellowship. TP and CAHA also acknowledge Direccíon General de Asuntos del Personal Académico (Project PAPIIT No. IN226310) for economic support. We acknowledge Director, IIT Ropar for constant encouragements.

References

1. Akin M, Prediger A, Yuksel M, Hopfner T, Demirkol DO, Beutel S, Timur S, Scheper T (2011) A new set up for multi-analyte sensing: at-line bio-process monitoring. Biosens Bioelectron 26:4532–4537
2. Tront JM, Fortner JD, Plotze M, Hughes JB, Puzrin AM (2008) Microbial fuel cell biosensor for in situ assessment of microbial activity. Biosens Bioelectron 24:586–590
3. Heller A, Feldman B (2008) Electrochemical glucose sensors and their applications in diabetes management. Chem Rev 108:2482–2505
4. Mano N, Heller A (2005) Detection of glucose at 2 fM concentration. Anal Chem 77:729–732
5. Lawrence NS, Deo RP, Wang J (2004) Biocatalytic carbon paste sensors based on a mediator pasting liquid. Anal Chem 76:3735–3739
6. Wang J (2008) Electrochemical glucose biosensors. Chem Rev 108:814–825
7. Anu Prathap MU, Thakur B, Sawant SN, Srivastava R (2012) Synthesis of mesostructured polyaniline using mixed surfactants, anionic sodium dodecylsulfate and non-ionic polymers and their applications in H_2O_2 and glucose sensing. Colloids Surf B 89:108–116
8. Anu Prathap MU, Chaurasia A, Sawant SN, Apte SK (2012) Polyaniline-based highly sensitive microbial biosensor for selective detection of lindane. Anal Chem 84:6672–6678
9. Anu Prathap MU, Kaur B, Srivastava R (2012) Hydrothermal synthesis of CuO micro-/nanostructures and their applications in the oxidative degradation of methylene blue and non-enzymatic sensing of glucose/H_2O_2. J Colloid Interface Sci 370:144–154
10. Ryu J, Kim K, Kim HS, Hahn HT, Lashmore D (2010) Intense pulsed light induced platinum–gold alloy formation on carbon nanotubes for non-enzymatic glucose detection. Biosens Bioelectron 26:602–607
11. Bai Y, Sun Y, Sun C (2008) Pt–Pb nanowire array electrode for enzyme-free glucose detection. Biosens Bioelectron 24:579–585
12. Yuan J, Wang K, Xia XH (2005) Highly ordered platinum-nanotubule arrays for amperometric glucose sensing. Adv Funct Mater 15:803–809
13. Willner I, Katz E (2000) Integration of layered redox proteins and conductive supports for bioelectronic applications. Angew Chem Int Ed 39:1180–1218
14. Heller A (1992) Electrical connection of enzyme redox centers to electrodes. J Phys Chem 96:3579–3587
15. Xiao F, Zhao F, Mei D, Mo Z, Zeng B (2009) Nonenzymatic glucose sensor based on ultrasonic-electrodeposition of bimetallic PtM (M = Ru, Pd and Au) nanoparticles on carbon nanotubes–ionic liquid composite film. Biosens Bioelectron 24:3481–3486
16. Fendler JH (1998) Nanoparticles and nanostructured films. Wiley-VCH, Weinheim
17. Fricker SP (1996) Medical uses of gold compounds: past, present and future. Gold Bull (Lond) 29:53–60
18. Fricker SP (2007) Metal based drugs: from serendipity to design. Dalton Trans 0:4903–4917

19. Hutchings GJ, Brust M, Schmidbaur H (2008) Gold—an introductory perspective. Chem Soc Rev 37:1759–1765
20. Mirkhalaf F, Schiffrin DJ (2010) Electrocatalytic oxygen reduction on functionalized gold nanoparticles incorporated in a hydrophobic environment. Langmuir 26:14995–15001
21. Jirkovsky JS, Halasa M, Schiffrin DJ (2010) Kinetics of electrocatalytic reduction of oxygen and hydrogen peroxide on dispersed gold nanoparticles. Phys Chem Chem Phys 12:8042–8052
22. Merchant B (1998) Gold, the noble metal and the paradoxes of its toxicology. Biologicals 26:49–59
23. Tominaga M, Shimazoe T, Nagashima M, Taniguchi I (2005) Electrocatalytic oxidation of glucose at gold nanoparticle-modified carbon electrodes in alkaline and neutral solutions. Electrochem Commun 7:189–193
24. Burke LD, Nugent PF (1997) The electrochemistry of gold. I. The redox behaviour of the metal in aqueous media. Gold Bull (Lond) 30:43–53
25. Burke LD, Nugent PF (1998) The electrochemistry of gold. II. The electrocatalytic behaviour of the metal in aqueous media. Gold Bull (Lond) 31:39–50
26. He X, Yam VW-W (2011) Luminescent gold(I) complexes for chemosensing. Coord Chem Rev 255:2111–2123
27. Kore R, Tumma M, Srivastava R (2012) Syntheses and catalytic activities of homogenous and hierarchical ZSM-5 grafted Pd(II) dicarbene complex of imidazole based ionic liquids. Catal Today 198:189–196
28. Catalano VJ, Etogo AO (2007) Preparation of Au(I), Ag(I), and Pd(II) N-heterocyclic carbene complexes utilizing a methylpyridyl-substituted NHC ligand. Formation of a luminescent coordination polymer. Inorg Chem 46:5608–5615
29. Ray L, Shaik MM, Ghosh P (2007) Air-stable, convenient to handle Pd based PEPPSI (pyridine enhanced precatalyst preparation, stabilization and initiation) themed precatalysts of *N*/*O*-functionalized N-heterocyclic carbenes and its utility in Suzuki–Miyaura cross-coupling reaction. Dalton Trans 4546:4555
30. Uson R, Laguna A, Laguna M (1989) (Tetrahydrothiophene) gold(I) or gold(III) complexes. Inorg Synth 26:85–91
31. Kunz PC, Kassack MU, Hamacher A, Spingler B (2009) Imidazole-based phosphane gold(I) complexes as potential agents for cancer treatment: synthesis, structural studies and antitumour activity. Dalton Trans 7741:7747
32. Catalano VJ, Malwitz MA, Etogo AO (2004) Pyridine substituted N-heterocyclic carbene ligands as supports for Au(I)–Ag(I) interactions: formation of a chiral coordination Polymer. Inorg Chem 43(5714):5724
33. Rios D, Olmstead MM, Balch AL (2009) Blue-, green- and non-luminescent crystals from one reaction. Isolation and structural characterization of a series of gold(I)–siver(I) heterometallic complexes utilizing a gold carbene metalloligand containing free amino groups. Inorg Chem 48(5279):5287
34. Tremiliosi-Filho G, Dall'Antonia LH, Jerkiewicz G (2005) Growth of surface oxides on gold electrodes under well-defined potential, time and temperature conditions. J Electroanal Chem 578:1–8
35. Burke LD, Buckley DT, Morrissey JA (1994) Novel view of the electrochemistry of gold. Analyst 119:841–845
36. Kuhlkamp P, Raubenheimer HG, Field JS, Desmet M (1998) Cyclic voltammetry of heterocyclic Au(I) and Au(III) carbene complexes. J Organomet Chem 552:69–74
37. Koelle U, Laguna A (1999) Electrochemistry of Au-complexes. Inorg Chim Acta 290:44–50
38. Wang J, Gong J, Xiong Y, Yang J, Gao Y, Liu Y, Lu X, Tang Z (2011) Shape-dependent electrocatalytic activity of monodispersed gold nanocrystals toward glucose oxidation. Chem Commun 47:6894–6896
39. Angerstein-Kozlowska H, Conway BE, Hamelin A, Stoicoviciu L (1987) Elementary steps of electrochemical oxidation of single-crystal planes of Au Part II. A chemical and structural basis of oxidation of the (111) plane. J Electroanal Chem 429:228–229
40. Bai Y, Yang W, Sun Y, Sun C (2008) Enzyme-free glucose sensor based on a three-dimensional gold film electrode. Sens Actuators B 134:471–476
41. Xu F, Cui K, Sun Y, Guo C, Liu Z, Zhang Y, Shi Y, Li Z (2010) Facile synthesis of urchin-like gold submicrostructures for non-enzymatic glucose sensing. Talanta 82:1845–1852
42. Bard AJ, Faulkner LR (2003) Electrochemical methods fundamentals and applications, 2nd edn. Wiley, Inc., New York
43. Nien P, Tung T, Ho K (2006) Amperometric glucose biosensor based on entrapment of glucose oxidase in a poly(3,4-ethylenedioxythiophene) film. Electroanalysis 18:1408–1415
44. Kawasaki T, Akanuma H, Yamanouchi T (2002) Increased fructose concentrations in blood and urine in patients with diabetes. Diabetes Care 25:353–357
45. Shamsipur M, Najafi M, Hosseini M-RM (2010) Highly improved electrooxidation of glucose at a nickel(II) oxide/multi-walled carbon nanotube modified glassy carbon electrode. Bioelectrochemistry 77:120–124
46. Mua Y, Jia D, Hea Y, Miaoa Y, Wu H-L (2011) Nano nickel oxide modified non-enzymatic glucose sensors with enhanced sensitivity through an electrochemical process strategy at high potential. Biosens Bioelectron 26:2948–2952
47. Nie H, Yao Z, Zhou X, Yang Z, Huang S (2011) Nonenzymatic electrochemical detection of glucose using well-distributed nickel nanoparticles on straight multi-walled carbon nanotubes. Biosens Bioelectron 30:28–34